Finite Elements in Analysis and Design 58 (2012) 20–30

Contents lists available at SciVerse ScienceDirect

Finite Elements in Analysis and Design

journal homepage: www.elsevier.com/locate/finel

Stress-based topology optimization using an isoparametric level set method

Kai A. James [a,*], Edmund Lee [a], Joaquim R.R.A. Martins [b]

[a] University of Toronto, Institute for Aerospace Studies, Toronto, Ontario, Canada
[b] University of Michigan, Department of Aerospace Engineering, Ann Arbor, MI, United States

ARTICLE INFO

Article history:
Received 4 July 2011
Received in revised form
19 March 2012
Accepted 20 March 2012
Available online 8 May 2012

Keywords:
Topology optimization
Level set method
Stress-based design
Von Mises stress
Finite element analysis
Isoparametric finite elements

ABSTRACT

This paper presents a novel framework for evaluating the shape sensitivities of the von Mises stress function using an isoparametric finite-element formulation. The use of the isoparametric formulation allows us to apply the level set method to structures that are confined to irregularly shaped domains and therefore must be modeled using body-fitted, nonuniform finite element meshes. The shape sensitivities of the von Mises stress function are evaluated on this nonuniform mesh and mapped isoparametrically to a uniform Cartesian grid on which the Hamilton–Jacobi equation is solved. The paper also introduces a new approach to the enforcement of volume constraints based on the augmented Lagrangian formulation. The method is demonstrated on a series of two-dimensional problems including an isoparametric variation of the classic *L-bracket* problem. We show that the isoparametric level set method produces converged, feasible designs whose performance is comparable to SIMP results in terms of their final objective value.

1. Introduction

The level set method (LSM) is a powerful tool for the shape and topology optimization of structures [1,2]. The large number of papers published on the topic in recent years attests to this. In spite of the increased popularity of LSM, most of the research devoted to it has focused on a small class of problems, while seeking to improve the numerical performance of the method [3–6]. Consequently, large classes of important problems have not yet been addressed. This is in contrast to more established methods such as SIMP [7], which have been applied to a wide variety of problems.

The current study focuses on two of these relatively unexplored areas. The first area involves the optimization of structures confined to irregularly shaped physical domains. In most level set studies, the example problems have a rectangle or a set of rectangles for the working domain. This type of region can easily be discretized into a uniform Cartesian mesh. However, when the region in which the optimized structure must lie is nonrectangular, as is the case for an aircraft wing for example [8], a uniform, rectilinear discretization is no longer possible. Instead, these problems require the use of nonuniform, body-fitted finite element meshes. Such problems are routinely solved by SIMP researchers [8–11], but they present a unique challenge for users of the level set method.

In level set optimization, the Hamilton–Jacobi equation, which describes the evolution of the material interface, is solved on a uniform Cartesian grid using a time-marching scheme. When the finite element mesh is uniform and rectilinear, the sensitivity information obtained in the finite element analysis can be passed directly into the Hamilton–Jacobi partial differential equation as a set of advection velocities.

Several authors have presented techniques for solving the Hamilton–Jacobi equation in problems where the finite element mesh is unstructured or simply nonuniform [12,13,6]. Often these methods involve constructing a piecewise continuous representation of the sensitivity field by interpolating the sensitivity values calculated at the Gauss points of the finite elements inside a region of interest. While these methods allow for the optimization of structures modeled using nonuniform, nonrectilinear meshes, they fail to address the situation in which the working domain of the problem is also nonrectangular. The isoparametric approach used in this study allows for the optimization of structures with contoured working domains, as is often the case in real-world engineering problems.

The isoparametric method was originally introduced by the first and third authors [14], and the current paper extends the method to stress-based design optimization, another area where the level set method has been relatively underused. We derive the discretized shape sensitivity formula for the von Mises stress function. Using the isoparametric method, we then map the resulting shape sensitivities to a uniform computational mesh on which the Hamilton–Jacobi equation is solved. The method is demonstrated on a series of example problems involving nonuniform, structured finite element meshes. The results are compared with several SIMP-

* Corresponding author. Tel.: +1 416 667 7747; fax: +1 416 667 7799.
E-mail address: kai.james@utoronto.ca (K.A. James).

0168-874X/$ - see front matter © 2012 Elsevier B.V. All rights reserved.
http://dx.doi.org/10.1016/j.finel.2012.03.012

based results to investigate the effectiveness of the isoparametric level set method for these problems.

2. Level set method

The level set method is used to optimize the location of a material boundary, which is defined implicitly as the zero contour of a higher-order function. The optimization problem can be formulated as follows:

$$\min_{\Omega} \quad J$$

$$\text{subject to} \quad c=0,$$

$$\mathbf{Kd}-\mathbf{F}=0,$$

$$\rho(x_i)=\begin{cases} 1, & x_i \in \Omega, \\ 10^{-3}, & x_i \in \overline{\Omega}, \end{cases}$$

$$\mathbf{k}(x)=\rho(x)\mathbf{k}_0, \tag{1}$$

where J is an objective function that depends on the design variable, Ω. In the results presented in subsequent sections, all structures are subject to a single equality constraint, c, on the structural volume. $\mathbf{K}$ is the global stiffness matrix, $\mathbf{d}$ is the vector of nodal displacements, and $\mathbf{F}$ is the vector of applied forces. The symbol ρ denotes the relative material density of the finite elements. This quantity determines the relative stiffness of each element via the element stiffness matrix $\mathbf{k}$. All elements located inside the solid region Ω are considered to have full density, and therefore $\rho=1$ for these elements. Elements lying outside the boundary are assigned a small nonzero density, ρ_{min}, to model the behavior of a void space without causing singularities in the global stiffness matrix. In the case of elements that are bisected by the structural boundary $\partial\Omega$, the relative material density is interpolated according to the portion of the element that lies within the boundary. All the material properties are assumed to be piecewise constant throughout each element.

The location of the material boundary, $\partial\Omega$, is represented implicitly through the level set function, ψ, which is defined via

$$\psi(x)=0; \; x \in \partial\Omega \cap D,$$

$$\psi(x)<0; \; x \in \Omega,$$

$$\psi(x)>0; \; x \in (D \cap \overline{\Omega}).$$

Fig. 1 shows an example of a level set function with the corresponding material boundary.

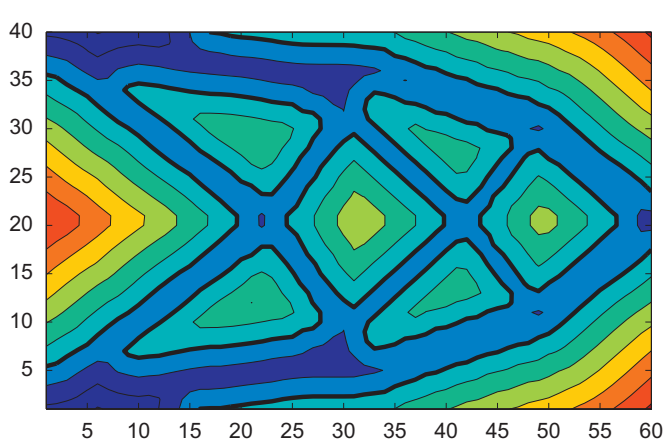

Fig. 1. Contour plot of optimized level set function with material boundary located at $\psi=0$ and represented by thick black line.

At each iteration, the level set function is updated using the Hamilton–Jacobi equation

$$\frac{\partial\psi}{\partial t}+v|\nabla\psi|=0 \Rightarrow \psi_{t+dt}=\psi_t-v|\nabla\psi_t|\,dt. \tag{2}$$

The term $\nabla\psi$ is computed numerically at each point in the computational grid by taking finite differences of the values of the level set function at adjacent nodes. The advection velocity v is determined by the shape sensitivity of the objective function at each point. The parameter t is a fictitious time parameter that represents the optimization iteration number, and the time step dt is chosen in such a way that the CFL condition is satisfied [15].

The level set function is initialized as the signed distance from the initial material boundary. After every few updates, the level set function is restored to its signed-distance form. Here we use an implementation of the fast sweeping method [16–18].

In accordance with the framework introduced by Allaire et al. [1], the shape sensitivities are given by the Fréchet functional derivative [19]

$$J'(\Omega)(\theta)=\int_{\partial\Omega} v\theta\cdot\mathbf{n}\,ds, \tag{3}$$

where θ is an arbitrary small vector field and $\mathbf{n}$ is the unit vector normal to the surface $\partial\Omega$. The value v provides the advection velocity at a given point on the boundary. For objective and constraint functions that depend on the displacement state u, the shape sensitivity is calculated using the adjoint method; a detailed derivation is presented by Allaire et al. [1]. For an arbitrary objective of the form

$$J(\Omega)=\int_{\Omega} j(x)\,dx+\int_{\partial\Omega} l(x)\,ds, \tag{4}$$

the generalized shape sensitivity is given by

$$J'(\Omega)(\theta)=\int_{\Omega} div(\theta(x)j(x))\,dx + \int_{\partial\Omega}\theta(x)\cdot\mathbf{n}(x)\left(\frac{\partial l(x)}{\partial\mathbf{n}(x)}+H(x)l(x)\right)ds, \tag{5}$$

$$\Rightarrow J'(\Omega)(\theta)=\int_{\partial\Omega}\theta(x)\cdot\mathbf{n}(x)j(x)\,ds + \int_{\partial\Omega}\theta(x)\cdot\mathbf{n}(x)\left(\frac{\partial l(x)}{\partial\mathbf{n}(x)}+H(x)l(x)\right)ds, \tag{6}$$

where H is the mean curvature of $\partial\Omega$.

3. Isoparametric formulation

The shape sensitivities shown in Section 2 assume a smooth, continuous displacement state u and strain field ϵ, which can be evaluated at any location in the working domain. In practice, the finite element method is used to generate a discrete representation of the displacement state, and the shape sensitivities are evaluated at the Gauss quadrature points for each element [5], or they can be averaged over the domain of the element, in which case the sensitivity is assumed to be piecewise constant across each element.

The shape sensitivity values derived above must be computed using finite element analysis, which produces a discretized approximation of the continuous sensitivity field. We evaluate the sensitivities at the Gauss quadrature points of each element [5] and then average these values to obtain a sensitivity field that is piecewise constant throughout each element. If the uniform finite element mesh is composed entirely of square or cubic elements, each finite element provides a unique advection velocity that can be used to update the Hamilton–Jacobi equation at each node in the computational mesh.

In contrast, with the isoparametric formulation, we can use arbitrary quadrilateral or hexahedral elements to perform the structural analysis. Isoparametric finite elements [20] allow us to retain the one-to-one mapping of advection velocities while allowing for nonuniform structural meshes. This makes it possible to model structures that are confined to nonrectangular or contoured domains. It also allows a designer to coarsen the structural mesh in regions of low material density or low strain and to refine the mesh in regions where the stress is likely to be high, thereby enhancing the computational efficiency of the algorithm.

The Hamilton–Jacobi equation is still solved using a uniform Cartesian grid, which is mapped to the nonuniform structural mesh shown in Fig. 2 using the Jacobian matrix of each finite element.

The Jacobian matrix, **J**, is defined to be

$$\mathbf{J}(\xi,\eta,\zeta)=\begin{bmatrix}\frac{\partial x}{\partial \xi} & \frac{\partial x}{\partial \eta} & \frac{\partial x}{\partial \zeta}\\ \frac{\partial y}{\partial \xi} & \frac{\partial y}{\partial \eta} & \frac{\partial y}{\partial \zeta}\\ \frac{\partial z}{\partial \xi} & \frac{\partial z}{\partial \eta} & \frac{\partial z}{\partial \zeta}\end{bmatrix}, \tag{7}$$

where the variables ξ, η, and ζ represent the local coordinates in each element, as shown in Fig. 3.

The relationship between the physical coordinates x, y, z and the local or *computational* coordinates ξ,η,ζ is determined by the element shape functions

$$x=\sum_{i=1}^{8} N_i(\xi,\eta,\zeta)x_i, \tag{8}$$

$$N_i(\xi,\eta,\zeta)=\frac{(1+\xi\xi_i)(1+\eta\eta_i)(1+\zeta\zeta_i)}{8}, \quad \xi_i,\eta_i,\zeta_i=\pm 1, \tag{9}$$

where N_i are the element shape functions and x_i are the coordinates of the element nodes. From this relationship, we can determine the precise correlation between the advection velocities calculated in physical space and those same velocities expressed in computational space.

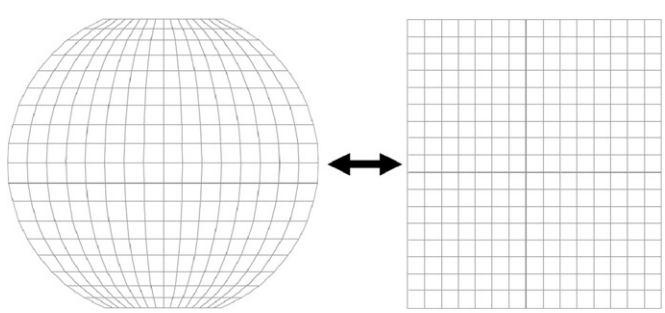

Fig. 2. Two-dimensional mapping of arbitrary structured mesh to uniform rectilinear computational mesh.

The advection velocities are chosen so that the vector composed of the magnitudes of all these velocities points in the direction of steepest descent. In a uniform volume field, the velocities depend only on the shape sensitivity of the objective or constraint function. However, in cases where the computational grid does not map uniformly into physical space, we must also take into consideration the contribution of this spatial mapping. Therefore, we introduce the concept of *relative impact*, which is a measure of the incremental change in the objective function caused by a shape perturbation at a given point on the material boundary. We define the relative impact μ at a point p as the product of the shape sensitivity at p and the incremental volume change caused by an infinitesimal shape perturbation at p.

An infinitesimal cube at point p in computational space can be assumed to have a volume of $d\xi\, d\eta\, d\zeta$. This cube represents a volume of $d\xi\, d\eta\, d\zeta|\mathbf{J}_p|$ in physical space. Therefore, the relative impact of a shape perturbation at p that results in an incremental volume change $d\xi\, d\eta\, d\zeta|\mathbf{J}_p|$ is given by

$$\mu_c=v_c\, d\xi\, d\eta\, d\zeta, \tag{10}$$

$$\mu_p=v_p\, d\xi\, d\eta\, d\zeta|\mathbf{J}_p|, \tag{11}$$

where v_p and v_c are the shape sensitivities at point p computed in physical space and computational space respectively. Noting that the relative impact must be consistent as we go from physical to computational space, we set $\mu_c=\mu_p$. Therefore, we get the following formula for the transformed computational advection velocities v_c given a set of shape sensitivities v_p:

$$v_c=v_p|\mathbf{J}_p|. \tag{12}$$

These velocities are then used in the solution of the Hamilton–Jacobian equation (2), because they represent the set of velocities that produce the maximum decrease in the objective function at a given time t.

Because the velocity field is modeled as being piecewise constant in each element, the conversion factor $|\mathbf{J}_p|$ is averaged over each element's volume. The resulting integral is equal to the element volume, which is given by

$$\mathrm{vol}_e=\int_{\Omega_e}\det(\mathbf{J}(\xi,\eta,\zeta))\, d\xi\, d\eta\, d\zeta. \tag{13}$$

Finally, we find that given some shape sensitivity, v_p, evaluated in physical space, the resulting advection velocity in computational space is given by $v_c=\mathrm{vol}_e v_p$.

3.1. Constitutive relation

The constitutive matrix, **D**, describes the relationship between the stress tensor, $\boldsymbol{\sigma}$, and the strain tensor, $\boldsymbol{\varepsilon}$, i.e.

$$\boldsymbol{\sigma}=\mathbf{D}\boldsymbol{\varepsilon}. \tag{14}$$

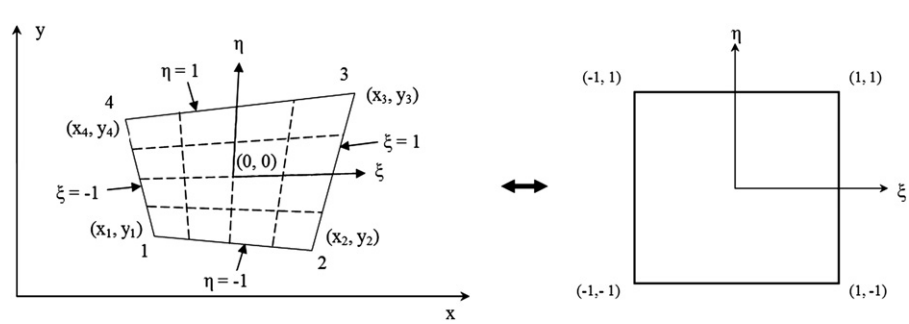

Fig. 3. Two-dimensional illustration of mapping from local to global coordinates for arbitrary quadrilateral element.

In the two-dimensional case, this relationship can be written

$$\begin{bmatrix} \sigma_{xx} \\ \sigma_{yy} \\ \sigma_{xy} \end{bmatrix} = \frac{E}{(1-\nu^2)} \begin{bmatrix} 1 & \nu & 0 \\ \nu & 1 & 0 \\ 0 & 0 & \frac{1-\nu}{2} \end{bmatrix} \begin{bmatrix} \varepsilon_{xx} \\ \varepsilon_{yy} \\ \varepsilon_{xy} \end{bmatrix}, \tag{15}$$

where E and ν are the Young's modulus and Poisson's ratio, respectively, of the isotropic material. In the examples presented, we use the *ersatz* material approach [1,21], in which the Young's modulus is scaled to account for void elements and elements that are bisected by the material boundary. For bisected elements, we interpolate the Young's modulus according to the portion of the element's volume that falls inside the boundary, i.e.

$$E_e = \rho_e E_0, \tag{16}$$

$$\Rightarrow \mathbf{D}_e = \rho_e \mathbf{D}_0, \tag{17}$$

where E_e is the *effective* Young's modulus of the element, and E_0 is the Young's modulus of the solid material. The relative material density ρ_e can be calculated as the fraction of the element's volume that lies inside the material boundary. Using the isoparametric formulation, we determine this quantity by the following integral [14]:

$$\rho_e = \frac{1}{\mathrm{vol}_e} \int_{\Omega_e} h(-\psi(\xi,\eta)) \det(\mathbf{J}(\xi,\eta))\, d\xi\, d\eta, \tag{18}$$

$$\rho_e \approx \frac{1}{\mathrm{vol}_e} \sum_{p}^{n_p} h(-\psi_p) |\mathbf{J}_p|. \tag{19}$$

The Heaviside function, h, is defined such that its value is unity where $\psi < 0$ (i.e., the solid region) and zero elsewhere. We evaluate this integral numerically, by dividing the element into a uniform grid of pixels. We set the number of pixels, n_p, to be greater than or equal to $1/\rho_{min}$. Each pixel is either *solid* or *void*, depending on the value of the level set function at that pixel's location, ψ_p. Therefore, the relative material density is approximated as a weighted sum of the Heavyside values for all the pixels in the element, with the weight given by the determinant of the Jacobian matrix. This operation can be computationally expensive, but the cost is mitigated by dividing the structural domain into blocks and carrying out the process in parallel.

3.2. Stress-based design

Stress-based design presents a challenge for practitioners of topology optimization. Because the stress function is local in nature, and because topology optimization involves large numbers of finite elements, the combination of these factors can result in thousands of individual constraints. An additional challenge is caused by the *singularity phenomenon* [22]. This issue was first encountered in truss optimization problems, where it was observed that as the thickness (which is analogous to material density) of an element approached zero, its stress value approached infinity, which prevented the full removal of extraneous elements. This resulted in degenerate subspaces in the feasible design space and caused most optimizers to converge to locally optimal designs. Users of the SIMP method have addressed this problem by relaxing the local stress constraints to smooth out the feasible design envelope [23,24].

While a significant amount of research has been devoted to stress-based topology optimization using the SIMP method, the problem of stress-based design remains largely unexplored by users of the level set method. One notable exception is the work of Allaire and Jouve [25]. They demonstrated that the level set method could indeed be used to effectively handle minimum stress design, while avoiding some of the numerical challenges associated with the SIMP method, including the stress singularity problem. More recently, Asmutz and Novotny [26] presented a new framework for the level set optimization of stress-based designs using the topological derivative [2].

The following section builds on the framework introduced by Allaire and Jouve [25] and extends it to incorporate isoparametric finite elements. As in [25] we use a variation of the p-norm function to aggregate the local von Mises stress values in each element. This procedure results in the global stress function

$$G = \int_{\Omega} \sigma_{VM}^{b}(x)\, dx, \tag{20}$$

where σ_{VM} is the local von Mises stress, and b is the aggregation parameter, which is some integer greater than 1.

The use of the p-norm function confers several advantages. In particular, it reduces the number of constraints from hundreds or thousands (at least one per element) to just one. This makes the optimization process more computationally efficient. Although the level set optimization method described above is designed to perform unconstrained optimization, a single constraint can be enforced simply by replacing the objective function with an augmented Lagrangian, as outlined in the following section.

The p-norm function provides a conservative approximation of the function $\max(\sigma_{VM_e})$, and so it can be used to enforce failure constraints or, as here, to minimize the maximum stress within a structure. The function can be made arbitrarily close to the *max* function by increasing the value of the exponent p. However, unlike the *max* function, the p-norm function is smooth, making it well-suited to gradient-based optimization. Care must be taken when selecting the value of the exponent p to balance the desire for a close approximation to the *max* function with the need to maintain a high degree of smoothness, to ensure the stability of the optimization process.

As shown by Allaire and Jouve [25], the shape derivative of this function is

$$G' = \int_{\partial\Omega} (\sigma_{VM}^{b}(x) + \boldsymbol{\varepsilon}^T(w(x)) \mathbf{D} \boldsymbol{\varepsilon}(u(x)))\, dx, \tag{21}$$

where $\boldsymbol{\varepsilon}^T(w(x))$ represents the strain tensor as a function of the adjoint state $w(x)$. We now derive the discretized formula for the isoparametric sensitivity field corresponding to the global von Mises stress formula (Eq. (20)), using Eq. (21) as our starting point.

As for the displacement state u, we solve for the adjoint state discretely at the nodes of the finite element mesh using Eq. (22). The adjoint field is then interpolated using the isoparametric shape functions given in Eq. (8)

$$\mathbf{K}\mathbf{w} = -\frac{\partial G}{\partial \mathbf{d}}. \tag{22}$$

In the above adjoint equation, $\mathbf{K}$ is the global stiffness matrix, obtained by summing the element stiffness matrices given in Eq. (23), and $\mathbf{d}$ is the global displacement vector, obtained by solving the governing equation, $\mathbf{K}\mathbf{d} - \mathbf{F} = \mathbf{0}$.

The element stiffness matrix is obtained by performing the following integral over the volume of the element:

$$\mathbf{k}_e = \int_{\Omega_e} \mathbf{B}^T(\xi,\eta) \mathbf{D}_e \mathbf{B}(\xi,\eta) |\mathbf{J}(\xi,\eta)|\, d\xi\, d\eta, \tag{23}$$

where the strain–displacement matrix, $\mathbf{B}$, is composed of the set of first derivatives of the element shape functions. It gives the relationship between the element nodal displacements and the strain tensor, ε, as shown below

$$\boldsymbol{\varepsilon}(\xi,\eta) = \mathbf{B}^T(\xi,\eta) \mathbf{d}_e. \tag{24}$$

The stress sensitivity is assumed to be piecewise constant across each element and is therefore approximated by averaging

the integrand of Eq. (21) over the domain of each element. The first term in the integrand is just the von Mises stress itself. The von Mises stress can be expressed in terms of the stress tensor as

$$\sigma_{VM}^2(\xi,\eta) = \sigma_{xx}^2 + \sigma_{xx}\sigma_{yy} + \sigma_{yy}^2 + 3\sigma_{xy}^2 \tag{25}$$

$$\sigma_{VM}^2(\xi,\eta) = \boldsymbol{\varepsilon}^T(\xi,\eta)\mathbf{DMD}\boldsymbol{\varepsilon}(\xi,\eta), \tag{26}$$

where $\mathbf{M}$ is the coefficient matrix

$$\mathbf{M} = \begin{bmatrix} 1 & -\frac{1}{2} & 0 \\ -\frac{1}{2} & 1 & 0 \\ 0 & 0 & 3 \end{bmatrix}, \tag{27}$$

as introduced by Svanberg and Werme [27]. Using finite elements, the discrete formula for the local von Mises stress at any point, $\{\xi,\eta\}$, is given by

$$\sigma_{VM}^2(\xi,\eta) = \mathbf{d}_e^T\mathbf{B}^T(\xi,\eta)\mathbf{DMDB}(\xi,\eta)\,\mathbf{d}_e. \tag{28}$$

To find the average of the local squared von Mises stress, we integrate over the domain of the element as follows:

$$\overline{\sigma_{VM}^2} = \frac{1}{\mathrm{vol}_e}\int_{\Omega_e} \mathbf{d}_e^T\mathbf{B}^T(\xi,\eta)\mathbf{DMDB}(\xi,\eta)\mathbf{d}_e|\mathbf{J}(\xi,\eta)|\,d\xi\,d\eta \tag{29}$$

$$\Rightarrow \overline{\sigma_{VM}^b} = \frac{1}{\mathrm{vol}_e}\int_{\Omega_e} (\mathbf{d}_e^T\mathbf{B}^T(\xi,\eta)\mathbf{DMDB}(\xi,\eta)\mathbf{d}_e)^{b/2}|\mathbf{J}(\xi,\eta)|\,d\xi\,d\eta. \tag{30}$$

We compute this integral using Gauss quadrature, yielding the following formula for the average von Mises stress:

$$\overline{\sigma_{VM}^b} = \frac{1}{\mathrm{vol}_e}\sum_i \omega_i(\mathbf{d}_e^T\mathbf{B}^T(\xi_i,\eta_i)\mathbf{DMDB}(\xi_i,\eta_i)\mathbf{d}_e)^{b/2}|\mathbf{J}(\xi_i,\eta_i)|. \tag{31}$$

Here $\{\omega_i\}$ are the Gauss weights and $\{\xi_i,\eta_i\}$ are the coordinates of the Gauss points. For compactness, we introduce the matrix $\mathbf{S}_i$, which is defined to be

$$\mathbf{S}_i = \mathbf{B}^T(\xi_i,\eta_i)\mathbf{DMDB}(\xi_i,\eta_i) \tag{32}$$

$$\Rightarrow \overline{\sigma_{VM}^b} = \frac{1}{\mathrm{vol}_e}\sum_i \omega_i(\mathbf{d}_e^T\mathbf{S}_{e_i}\mathbf{d}_e)^{b/2}|\mathbf{J}(\xi_i,\eta_i)|. \tag{33}$$

Note that because this matrix is dependent on the constitutive matrix, $\mathbf{D}$, it scales quadratically with the relative material density ρ.

Moving now to the second term in the formula for the global von Mises stress (Eq. (21)), we can express the product $\boldsymbol{\varepsilon}^T(w(x))\mathbf{D}\boldsymbol{\varepsilon}(u(x))$ in terms of the element stiffness matrix and the element displacement and adjoint vectors, $\mathbf{d}_e$ and $\mathbf{w}_e$ respectively. Using Gauss quadrature integration, we obtain the following discrete expression for the element stiffness matrix:

$$\mathbf{k}_e = \sum_i \omega_i(\mathbf{d}_e^T\mathbf{B}^T(\xi_i,\eta_i)\mathbf{DB}(\xi_i,\eta_i)\mathbf{d}_e)^{b/2}|\mathbf{J}(\xi_i,\eta_i)|. \tag{34}$$

Combining Eq. (23) with Eq. (24) gives

$$\int_{\Omega_e} \boldsymbol{\varepsilon}^T(w(x))\mathbf{D}\boldsymbol{\varepsilon}(u(x)) = \mathbf{w}_e^T\mathbf{k}_e\mathbf{d}_e. \tag{35}$$

To solve for the adjoint state, $\mathbf{w}$, we first write the finite element approximation of the global stress function G in terms of the element nodal displacement vectors $\mathbf{d}_e$, the element adjoint vectors $\mathbf{w}_e$, and the matrices, $\mathbf{S}_{e_i}$, calculated for each element

$$G = \sum_e (\mathrm{vol}_e\overline{\sigma_{VM_e}^b}) \tag{36}$$

$$= \sum_e\sum_i (\omega_i(\mathbf{d}_e^T\mathbf{S}_{e_i}\mathbf{d}_e)^{b/2}|\mathbf{J}_e(\xi_i,\eta_i)|). \tag{37}$$

Taking the first derivative of this equation with respect to $\mathbf{d}_e$ we obtain an expression for the right-hand side of the adjoint equation (Eq. (22)). Using the Gauss quadrature approximation of the global von Mises stress function shown above, we can find the partial derivative analytically

$$\frac{\partial G}{\partial \mathbf{d}_e} = \sum_i |\mathbf{J}_e(\xi_i,\eta_i)|(\omega_i b(\mathbf{d}_e^T\mathbf{S}_{e_i}\mathbf{d}_e)^{(b/2)-1}\mathbf{S}_i)\mathbf{d}_e. \tag{38}$$

Substituting this vector into Eq. (22) and solving for the adjoint vector, $\mathbf{w}$, we can now write the expression for the advection velocity v_p of each element. Taking the integrand of the shape sensitivity function (Eq. (21)), we express the advection velocity in discrete form by

$$v_p = \frac{1}{\mathrm{vol}_e}\left(\sum_i \omega_i(\mathbf{d}_e^T\mathbf{S}_{e_i}\mathbf{d}_e)^{b/2}|\mathbf{J}_e(\xi_i,\eta_i)| + \mathbf{w}_e^T\mathbf{k}_e\mathbf{d}_e\right). \tag{39}$$

This value can be converted to its equivalent in computational space by multiplying by a factor of vol_e. Therefore, the final computational advection velocity, v_c, for the global von Mises stress function is given by

$$v_c = \sum_i \omega_i(\mathbf{d}_e^T\mathbf{S}_{e_i}\mathbf{d}_e)^{b/2}|\mathbf{J}_e(\xi_i,\eta_i)| + \mathbf{w}_e^T\mathbf{k}_e\mathbf{d}_e. \tag{40}$$

During each iteration of the optimization algorithm, this function is computed for each element, with the resulting values being passed into the Hamilton–Jacobi equation (Eq. (2)) to update the level set function.

4. Constraint handling

The enforcement of constraints in optimization problems is typically achieved using a Lagrange-multiplier approach. However, in many level set schemes, the Lagrange multiplier is replaced by a constant coefficient, so that the task is to optimize a weighted sum of the objective and constraint functions [1]. Others perform a line search to determine the value of the Lagrange multiplier that satisfies the constraint at each iteration [5]. The weighted-sum approach is imprecise; it offers the designer no control over the final value of the constraint function. However, the line-search approach requires the repeated evaluation of the volume constraint function at each major optimization iteration. Even the evaluation of a volume constraint can be computationally expensive when isoparametric elements are used. To address these issues, we have developed an adaptive Lagrangian approach that strictly enforces the constraint and requires only one evaluation of the constraint function at each major iteration.

We define the Lagrangian $\mathcal{L}$ as a weighted sum of the objective function, G, and the constraint function, c, which, in this case, is the structural volume. The Lagrange multiplier λ acts as the weight coefficient in the summation expression

$$\mathcal{L} = G(\Omega) + \lambda c(\Omega). \tag{41}$$

We then perform unconstrained optimization of the Lagrangian with respect to the design variable Ω. At each iteration, the Lagrangian is updated using the heuristic

$$\lambda_{k+1} = \lambda_k + rc(\Omega). \tag{42}$$

This update corresponds to a descent step, whose length is given by the derivative of the Lagrangian with respect to λ, as well as the step size r, which is chosen to obtain an acceptable trade-off between convergence time and stability. In the results presented this method yielded converged solutions in which the final constraint value was within 0.01% of the target value.

5. Numerical examples

The isoparametric stress formulation derived above is demonstrated on a series of benchmark problems, which are based on a variation of the L-bracket problem. The initial design and loading conditions are shown in Fig. 4. The finite element mesh is composed of a grid of trapezoidal elements, shown in Fig. 5, so that it can be mapped to a single rectangular Cartesian mesh. The mesh is finest along the inner surface of the structure where the entrant corner appears and where the local von Mises stress is likely to be highest. The elements along the outer surface (i.e., the left and bottom edges of the vertical and horizontal segments respectively) are slightly larger and have a higher aspect ratio.

In our examples, we minimize the global von Mises stress while enforcing a 40% volume constraint. The problem is solved for two different values of the aggregation parameter b. Fig. 6 shows the material boundaries for the optimized structures corresponding to the two objective functions. The solutions in Fig. 6 contain some areas where the material boundary appears to be non-smooth. This is caused by the inexactness of the method used for computing the shape sensitivities, as well as the inexactness of the method used for plotting the material boundary. Because the boundary location is approximated using a limited amount of discrete data, this can introduce some imperfections. However, these imperfections have a minimal impact on the material density distribution (shown in Fig. 7), which is ultimately what determines the stress distributions. The stress distributions for the $b=2$ and $b=6$ solutions are shown in Figs. 8 and 9 respectively.

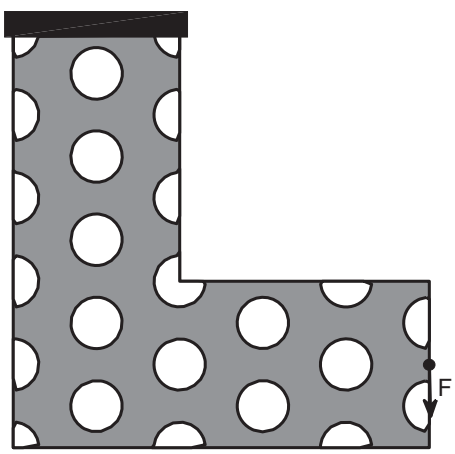

Fig. 4. Initial design and boundary conditions for L-bracket problem.

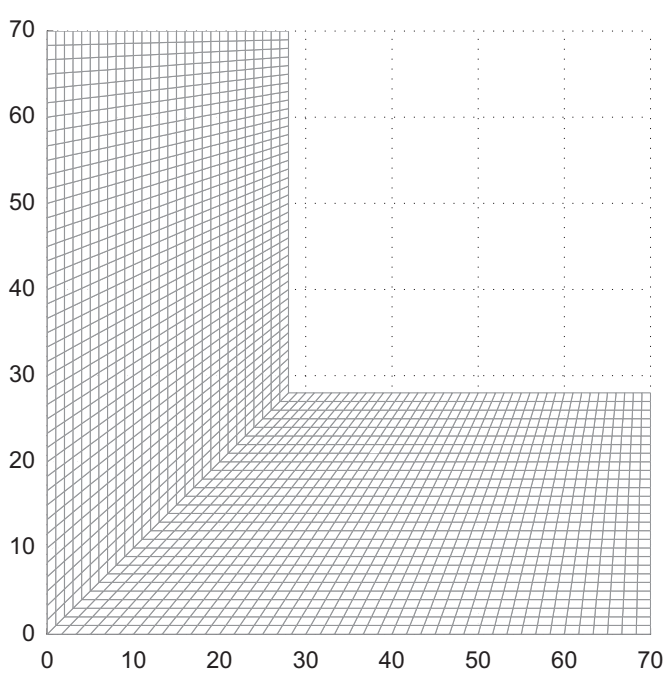

Fig. 5. Trapezoidal finite element mesh used in L-bracket problem.

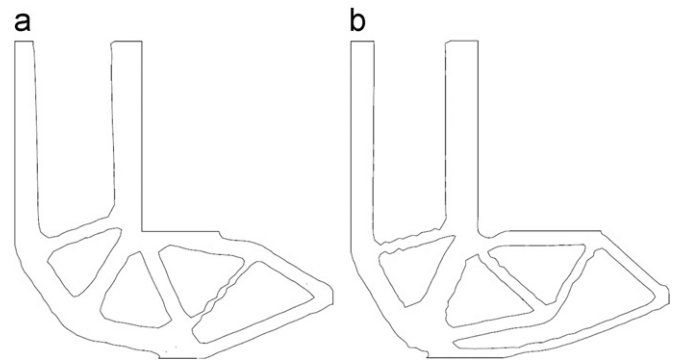

Fig. 6. Optimized structures for L-bracket with minimum global von Mises stress. Each figure shows contour line $\psi=0$ of optimized level set function. (a) $b=2$. (b) $b=6$.

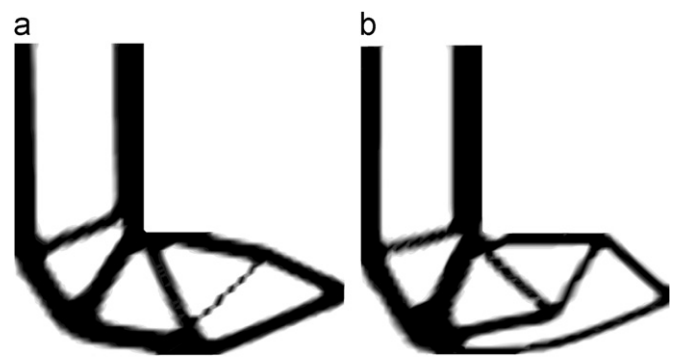

Fig. 7. Material distributions for the minimum-stress L-bracket structures. (a) $b=2$. (b) $b=6$.

It is often the goal of stress-based design to minimize the maximum local von Mises stress in the structure [23]. To do this, we may set the aggregation parameter, b, to some integer value that is large relative to the number of finite elements, since, in the limit as b approaches infinity, the p-norm aggregate is equivalent to the function $\max\{\sigma_e\}$. However, we are restricted in our choice of values for b. If b is too large, the elements with high stress dominate the sensitivity field, and the contribution from low-stress elements approaches zero. Therefore, to maintain the stability of the algorithm, b is chosen such that $b \ll n_e$, where n_e is the number of finite elements in the structure.

In spite of this, we see that even at low values of the aggregation parameter, the algorithm seeks to reduce the presence of stress concentrations. In the case where $b=6$, the stress concentration caused by the re-entrant corner dominates the global von Mises stress function. Therefore, rather than filling in the void at this location (which maximizes stiffness), the optimizer retains a smooth curve that dissipates the stress concentration and lowers the maximum local stress. However, it is important to begin the optimization with some material interface near the location of the entrant corner. In the above example, this requirement is satisfied by keeping the entrant corner void in the initial design. The reason for this approach is that the optimizer uses sensitivity information

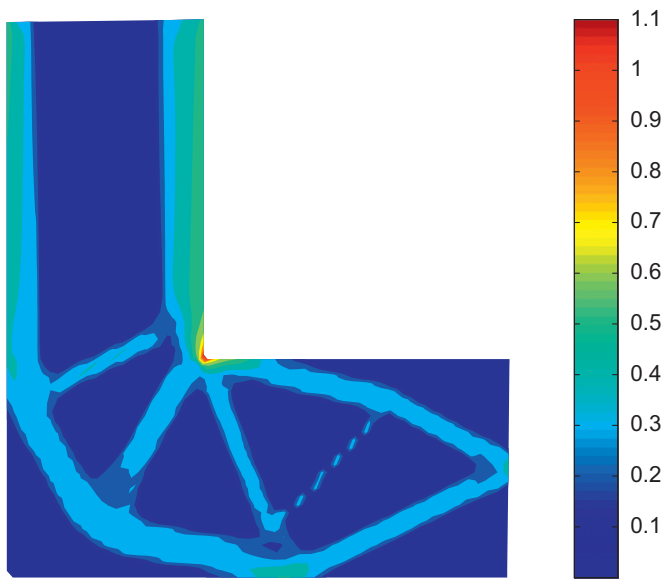

Fig. 8. Local von Mises stress distribution for $b=2$ showing spike in stress at entrant corner.

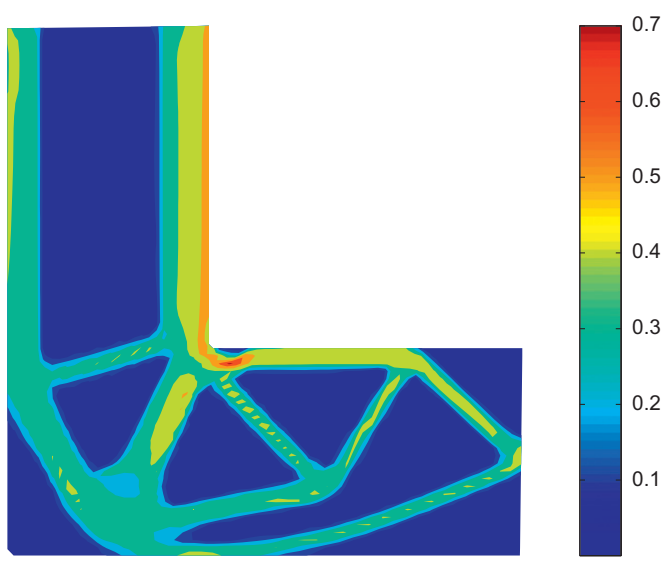

Fig. 9. Local von Mises stress distribution for $b=6$.

only along the material boundary (which is not to be confused with the *domain* boundary), and it can generate changes in the structure only through movement of the material boundary. Therefore, if the entire region near the stress concentration is solid, the entrant corner is likely to remain sharp with a high stress concentration because there is no nearby material interface that can be used to reshape the structure at this location. In this sense, the optimized structure is dependent on the initial design.

Figs. 10 and 11 show the convergence histories of the global von Mises stress function and the volume constraint for the L-bracket optimization problem. The plots show that the adaptive Lagrangian method for handling constraints produces some overshoot, but it ultimately converges to an optimal solution in which the constraint is satisfied. The convergence history of the $b=6$ case demonstrates the impact of the aggregation parameter p, which must be chosen carefully. Near the beginning of the optimization, we observe mild oscillations in the global von Mises stress value. As the aggregation parameter increases, the number and magnitude of these oscillations also increase because of a

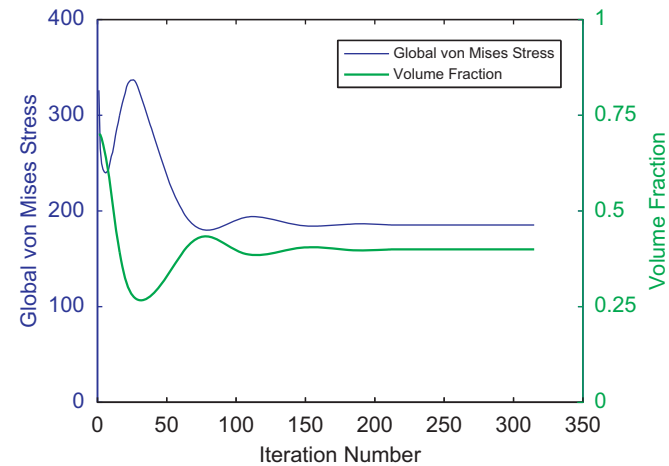

Fig. 10. Convergence history of objective and constraint functions for minimum-stress L-bracket problem with $b=2$.

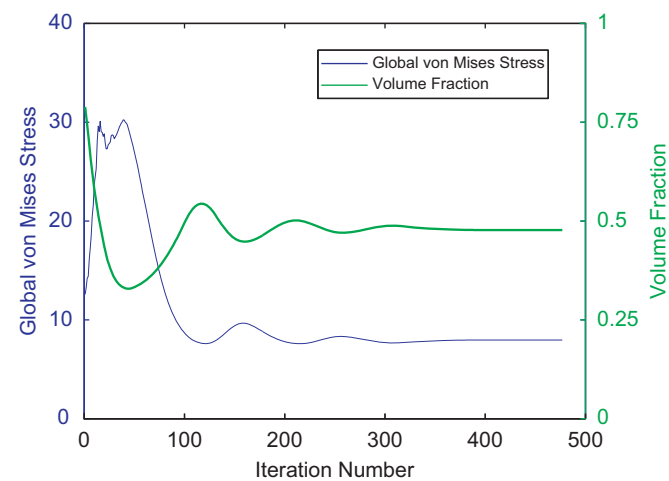

Fig. 11. Convergence history of objective and constraint functions for minimum-stress L-bracket problem with $b=6$.

Table 1
Comparison of L-bracket solutions optimized for various objectives.

Optimized for	Optimization result			
	$\sum\sigma^2$	$\sum\sigma^6$	$\max\{\sigma\}$	Comp.
$\sum\sigma^2$	184.75	33.621	1.146	197.11
$\sum\sigma^6$	194.38	7.951	0.715	218.90
Comp.	182.23	29.594	1.104	192.96

decrease in the degree of smoothness in the global von Mises stress function, which can prolong or prevent convergence.

Table 1 contains a breakdown of the numerical results for each case. In the table each row corresponds to a different solution optimized for a specific objective. The columns represent the different performance criteria used to evaluate each solution. The table shows that each solution is designed to perform well for its specific objective. The table also compares the stress-based results with those of an L-bracket optimized using the same mesh and boundary conditions but with compliance as the objective function (Figs. 12 and 13). The numbers reveal that the minimum-compliance bracket exhibits good global stress behavior for low values of the aggregation parameter. However, for higher values of b, the global von Mises stress is dominated by regions of highly concentrated stress, and in these cases the global stress

formulation works best. This is illustrated by column 3 of the table, which shows the maximum local stress in the structure. In this category, the stress-based formulation with $b=6$ performs the best.

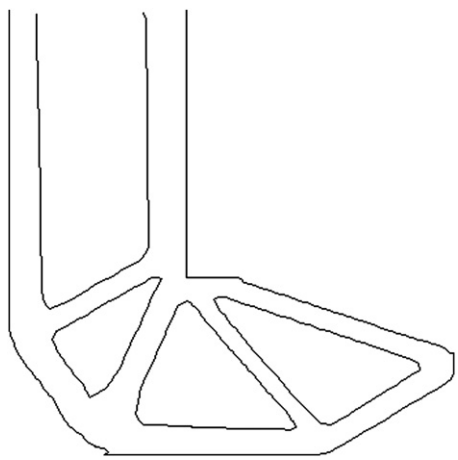

Fig. 12. Optimized material boundary for minimum-compliance L-bracket.

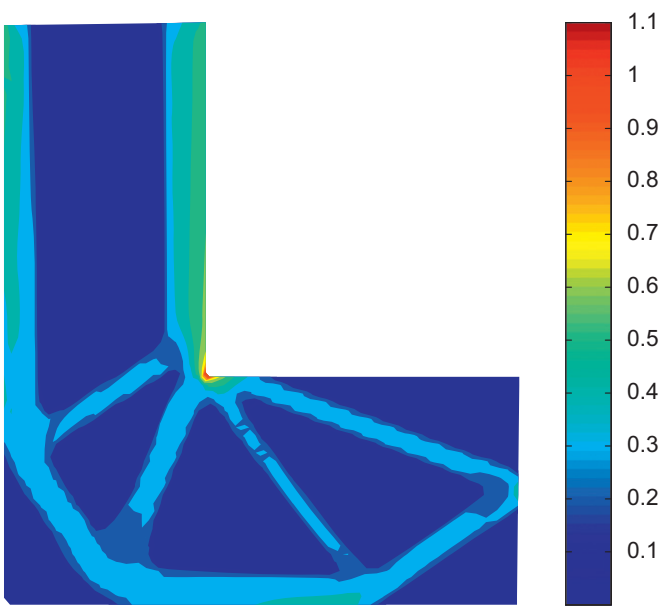

Fig. 13. Local von Mises stress distribution for minimum-compliance L-bracket.

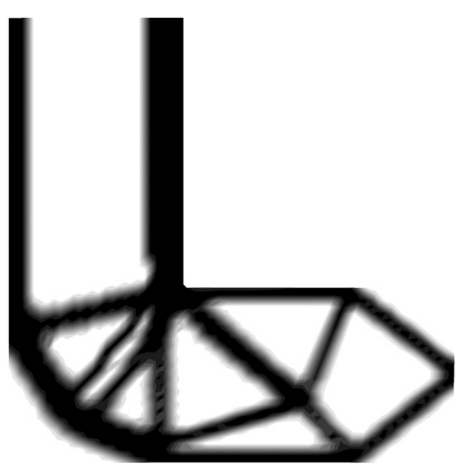

Fig. 14. SIMP solution for minimum-stress L-bracket with $b=6$.

The results shown in Fig. 6 were also compared with the results obtained using a SIMP formulation. To compare the two methods, we performed the SIMP optimization using the finite

Table 2
Comparison of optimized objective values of level set and SIMP solutions for minimum-stress L-bracket problem.

Method	$\sum \sigma^2$	$\sum \sigma^6$
Level set	184.75	7.95
SIMP	206.28	11.63

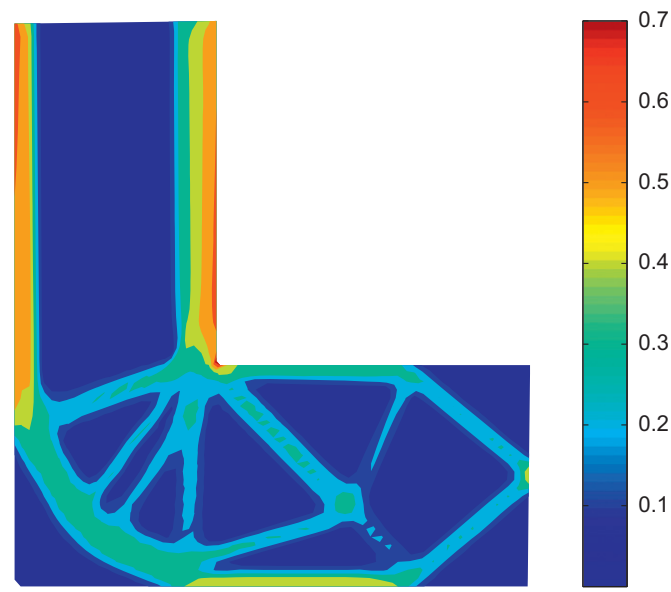

Fig. 15. Local von Mises stress distribution for minimum-stress SIMP solution with $b=6$.

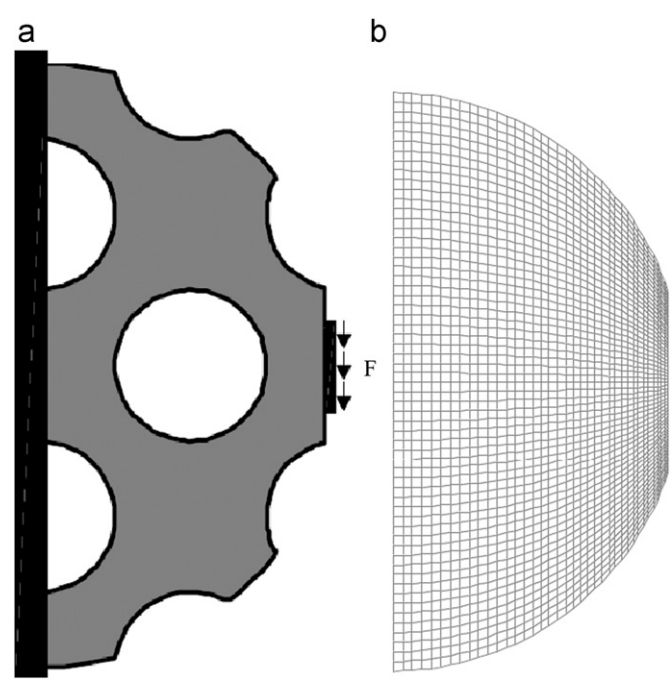

Fig. 16. Semicircular cantilever beam problem. (a) Loads and constraints and (b) finite element mesh.

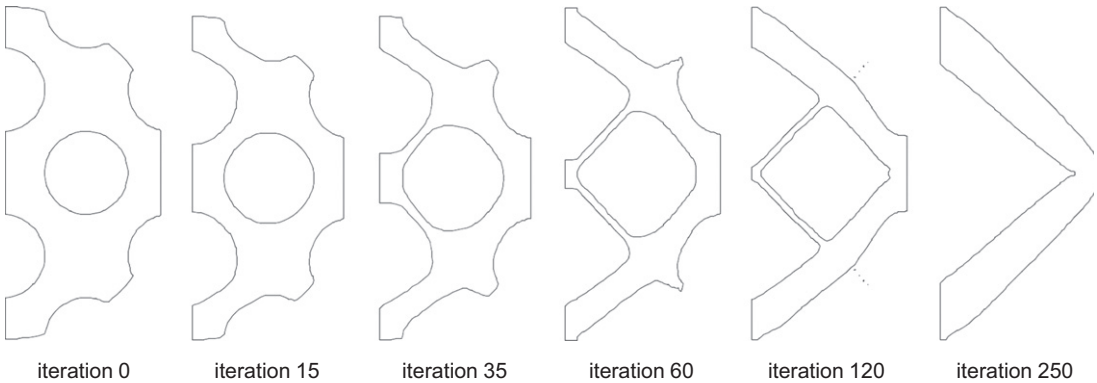

Fig. 17. Semicircular cantilever beam at various stages of optimization.

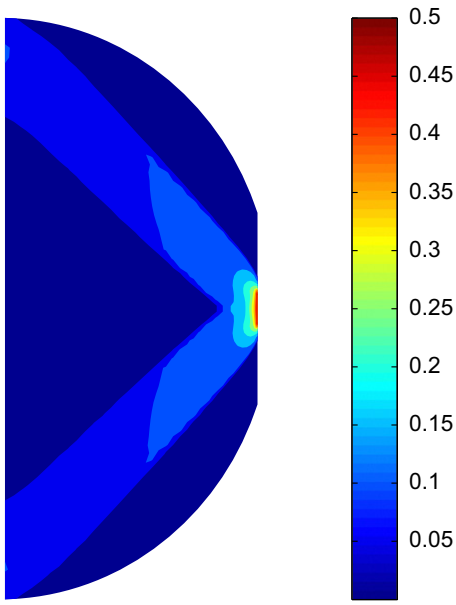

Fig. 18. Local von Mises stress distribution for semicircular cantilever beam.

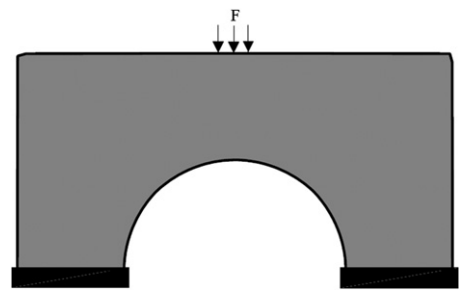

Fig. 19. Geometry and boundary conditions for isoparametric bridge problem.

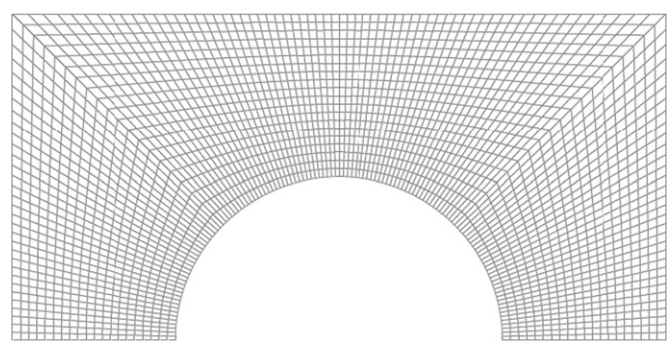

Fig. 20. Finite element mesh used in isoparametric bridge problem.

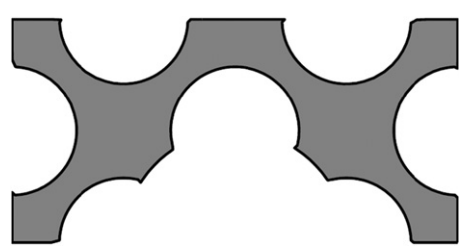

Fig. 21. Initial shape and topology of bridge structure.

element mesh shown in Fig. 5 with the relaxed p-norm formulation introduced by Le et al. [28]. To eliminate the checkerboarding that can occur with bilinear SIMP-type elements, we used a node-based density formulation, in which C^0 continuity of the density field was enforced across the elements [29,30].

Fig. 14 shows the SIMP solution for the case where the aggregation parameter is set to $b=6$. The corresponding von Mises stress distribution is shown in Fig. 15. Table 2 shows a comparison of the performances of the level set solutions and the SIMP solutions in terms of their objective values. The table shows that the level set solutions slightly outperform the SIMP solutions in both cases. This indicates that the isoparametric level set method is competitive with the SIMP method in terms of the performance of the optimized structures, but it does not conclusively demonstrate the superiority of the former method. It should also be noted that although the re-entrant corner has not been eliminated in the SIMP solution in this particular case, this result will differ at higher values of the aggregation parameter p. For such values, as shown in Table 1, stress concentrations dominate the global von Mises stress function and drive the optimization search.

In addition to allowing for a locally refined finite element mesh, the isoparametric formulation allows us to apply the level set method to structures with nonrectangular domains, as is the case in many real-world engineering problems. The following examples show how the isoparametric stress formulation can be used to optimize a structure whose working domain is nonrectangular. The first example is that of a short cantilever beam with a semicircular domain. Fig. 16(a) shows the initial design and boundary conditions for the problem. To model this problem, we use the semicircular finite element mesh shown in Fig. 16(b). In this problem, as in the previous examples, the objective is to minimize the global stress function (36), subject to a 40% constraint on the final volume fraction. The aggregation parameter is set to $b=6$.

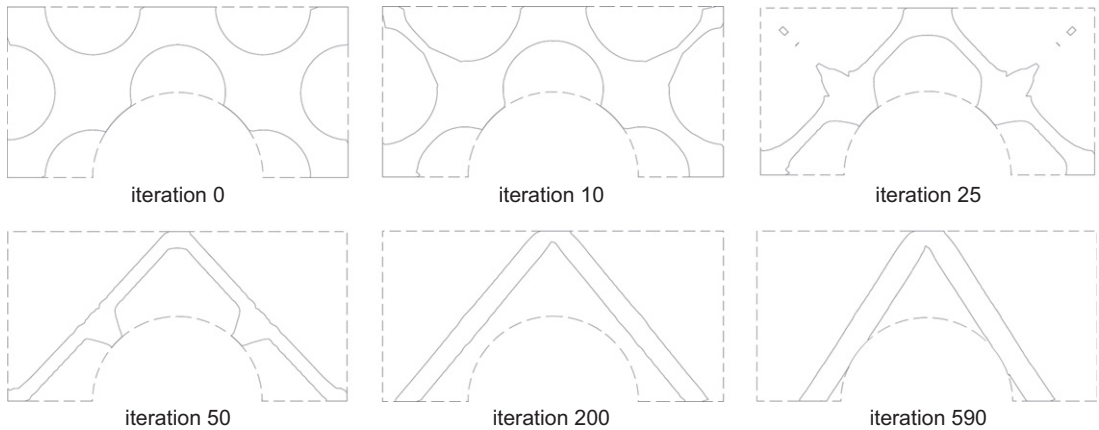

Fig. 22. Material boundary of bridge structure at various stages of optimization.

Fig. 17 shows the location of the material boundary at various stages of the optimization process. The final image contains the optimized structure, which is composed of two members that converge at a 90° junction to form a symmetric truss structure. Fig. 18 shows the von Mises stress distribution in the optimized structure together with the working domain for the problem.

In the second example we use the isoparametric formulation to optimize a bridge structure whose geometry and loading conditions are given in Fig. 19. Material can be placed anywhere in the grey region. The structure is clamped along the bottom surface, while a narrow uniform distributed load is applied to the top of the structure. This example, like the semicircular cantilever beam example, highlights the usefulness of the isoparametric level set method. The curved portions of domain boundaries for both problems are most effectively handled using a body-fitted mesh. Although it is possible to handle this problem using a uniform Cartesian mesh, a large number of much smaller elements would be needed to fit the Cartesian finite element mesh to the curvature of the domain boundary. Furthermore, one would have to expend significant effort to keep track of the element numbering when traversing the finite element mesh in order to perform the Hamilton–Jacobi update, as the computational mesh would no longer be rectangular. The isoparametric level set method circumvents both these challenges with little additional computational or development cost.

Figs. 20 and 21 show the finite element mesh and the initial design of the structure. The problem is solved for minimum global von Mises stress subject to a 20% constraint on the final volume fraction.

Fig. 22 shows the location of the material boundary at various stages of the optimization. The dashed line represents the domain boundary. The final image (iteration 590) depicts the optimized structure. Note that the structure initially converges rapidly toward the two-member truss configuration. Then, beginning around iteration 50, the two members begin to migrate inward toward the edge of the semicircular void. The optimization progresses relatively fast initially but slows down significantly as the design approaches an optimum and the advection velocities approach zero.

It should also be noted that in both the cantilever beam problem and the bridge problem, there is no stress concentration at the bottom of the junction where the two members meet. This is because of the clamped boundary condition at the base of both structures. This boundary condition prevents the members from moving outward, so there is no internal moment in the structure at the junction point. As a result, we do not see the entrant-corner effect that was present in the L-bracket problem.

6. Conclusions

We have presented a method for the design of structures modeled using nonuniform finite element meshes and optimized for minimum von Mises stress. The method was demonstrated on a series of examples based on the classical L-bracket problem and shown to produce converged, feasible designs. This result is significant in that it applies level set optimization to two classes of problems that have been largely unexplored by researchers investigating the level set method. The ability to use nonuniform finite element meshes is important because it vastly increases the range of problems to which the level set method can be applied. Additionally, the technique can be used to improve the computational efficiency of existing algorithms since it allows users to strategically refine the mesh in regions of interest. The problem of stress-based design in the context of the level set method is another area that receives little attention despite its usefulness. The combination of the isoparametric method with von Mises stress constraints provides a useful tool for the design of practical structures that can be used in real-world applications.

Acknowledgments

This research was partially supported by the Ontario Graduate Scholarship program.

References

[1] G. Allaire, F. Jouve, A.-M. Toader, Structural optimization using sensitivity analysis and a level-set method, J. Comput. Phys. 194 (1) (2004) 363–393.
[2] M. Burger, B. Hackl, W. Ring, Incorporating topological derivatives into level set methods, J. Comput. Phys. 194 (2004) 344–362.
[3] G. Allaire, F. Jouve, F. de Gournay, A.-M. Toader, Structural optimization using topological and shape sensitivity via a level set method, Control Cybern. 34 (2005) 59–80.
[4] F. de Gournay, Velocity extension for the level-set method and multiple eigenvalues in shape optimization, SIAM J. Control Optim. 45 (1) (2006) 343–367.
[5] S. Wang, K. Lim, B. Khoo, M. Wang, An extended level set method for shape and topology optimization, J. Comput. Phys. 221 (1) (2007) 395–421.
[6] P. Dunning, H. Kim, Investigation and improvement of sensitivity computation using the area-fraction weighted fixed grid FEM and structural optimization, Finite Elem. Anal. Des. 47 (2011) 933–941.
[7] G.I.N. Rozvany, M. Zhou, T. Birker, Generalized shape optimization without homogenization, Struct. Multidiscip. Optim. 4 (1992) 250–252.

[8] L. Krog, A. Tucker, Topology optimization of aircraft wing box ribs, in: 10th AIAA/ISSMO Multidisciplinary Analysis and Optimization Conference, Albany, NY, 2004, AIAA Paper 2004-4481.
[9] T.H. Lee, S.Y. Han, J.K. Lim, Topology optimization of the inner reinforcement for an automobile hood using modal design sensitivity analysis, Key Eng. Mater. 183–187 (2000) 439–444.
[10] D.-F. Wang, B. Zhang, J. Chen, S.-P. Wang, S.-Q. Liu, Application of topology optimization to commercial vehicle cab design, in: International Conference on Measuring Technology and Mechatronics Automation, vol. 2, Zhangjiajie, Hunan, China, 2009, pp. 763–766.
[11] J.-F. Shi, J.-H. Sun, Overview on innovation of topology optimization in vehicle CAE, in: 2009 International Conference on Electronic Computer Technology, 2009, pp. 457–460.
[12] S.-H. Ha, S. Cho, Level set based topological shape optimization of geometrically nonlinear structures using unstructured mesh, Comput. Struct. 86 (13–14) (2008) 1447–1455.
[13] Z. Liu, J.G. Korvink, Adaptive moving mesh level set method for structure topology optimization, Eng. Optim. 40 (6) (2008) 529–558.
[14] K. James, J.R. Martins, An isoparametric approach to level set topology optimization using a body-fitted finite element mesh, Comput. Struct. 90–91 (2012) 97–106.
[15] S. Wang, M.Y. Wang, A moving superimposed finite element method for structural topology optimization, Int. J. Numer. Methods Eng. 65 (2006) 1892–1922.
[16] J.A. Sethian, A fast marching level set method for monotonically advancing fronts, in: Proc. Natl. Acad. Sci. (1995) 1591–1595.
[17] T. Oberhuber, Numerical recovery of the signed distance function, in: Czech-Japanese Seminar in Applied Mathematics, Prague, Czech Republic, 2004, pp. 148–164.
[18] Y.R. Tsai, L. Cheng, S. Osher, H. Zhao, Fast sweeping algorithms for a class of Hamilton–Jacobi equations, SIAM J. Numer. Anal. 41 (2003) 673–694.
[19] J. Simon, Differentiation with respect to the domain in boundary value problems, Numer. Funct. Anal. Optim. 2 (1980) 649–687.
[20] B.M. Irons, Engineering applications of numerical integration in stiffness methods, AIAA J. 4 (11) (1966) 2035–2037.
[21] Z. Luo, L. Tong, Z. Kang, A level set method for structural shape and topology optimization using radial basis functions, Comput. Struct. 87 (7–8) (2009) 425–434.
[22] G.D. Cheng, Z. Jiang, Study on topology optimization with stress constraints, Eng. Optim. 190 (26–27) (1992) 3443–3459.
[23] P. Duysinx, M.P. Bendse, Topology optimization of continuum structures with local stress constraints, Int. J. Numer. Methods Eng. 43 (8) (1998) 1453–1478.
[24] G.D. Cheng, X. Guo, Epsilon-relaxed approach in structural topology optimization, Struct. Multidiscip. Optim. 13 (4) (1997) 258–266.
[25] G. Allaire, F. Jouve, Minimum stress optimal design with the level set method, Eng. Anal. Bound. Elem. 32 (11) (2008) 909–918.
[26] S. Asmutz, A. Novotny, Topological optimization of structures subject to von Mises stress constraints, J. Comput. Phys. 41 (3) (2009) 407–420.
[27] K. Svanberg, M. Werme, Sequential integer programming methods for stress-constrained topology optimization, Struct. Multidiscip. Optim. 34 (4) (2007) 288–299.
[28] C. Le, J. Norato, T. Bruns, C. Ha, D. Tortorelli, Stress-based topology optimization for continua, Struct. Multidiscip. Optim. 41 (2010) 605–620.
[29] C. Jog, R. Haber, Stability of finite element models for distributed-parameter optimization and topology design, Comput. Methods Appl. Mech. Eng. 130 (1996) 203–226.
[30] G.I.N. Rozvany, M. Zhou, T. Birker, A q4/q4 continuum structural topology optimization implementation, Struct. Multidiscip. Optim. 27 (2003) 130–135.